

Oncogenic role and target properties of the lysine-specific demethylase KDM1A in chronic lymphocytic leukemia

Qu Jiang, Johanna Stachelscheid, Johannes Bloehdorn, Alicja Pacholewska, Christoph Aszyk, Francien Grotenhuijs, Tony Müller, Alicja Pacholewska, Ozlem Onder, Prerana Wagle, Carmen D. Herling, Maria Kleppe, Zhefang Wang, Kevin R. Coombes, Sandra Robrecht, Priya S. Dalvi, Bianca Plosnita, Petra Mayer, Lynne V. Abruzzo, Janine Altmüller, Birgit Gathof, Thorsten Persigehl, Kirsten Fischer, Billy Jebaraj, Hugh Y Rienhoff, Rupert Ecker, Yue Zhao, Christiane J. Bruns, Stephan Stilgenbauer, Kojo Elenitoba-Johnson, Michael Hallek, Michal R. Schweiger, Margarete Odenthal, Elena Vasyutina, and Marco Herling

SUPPLEMENTAL FIGURES AND METHODS

CONTENTS

1 Supplemental Figures

Supplemental Figure 1-6

2 Supplemental Methods

Isolation of B-cells from tonsils

Animal experiments

Isolation of murine splenic mononuclear cells and bone marrow cells

Tissue cytometry

Cell culture

Constructs

Transfection and transduction

Proliferation assay

Demethylase activity assay

MTS assay

Chromatin immunoprecipitation sequencing (ChIP-seq)

Quantitative real-time PCR (qRT-PCR)

Mass spectrometry (MS)

Analysis of MS data

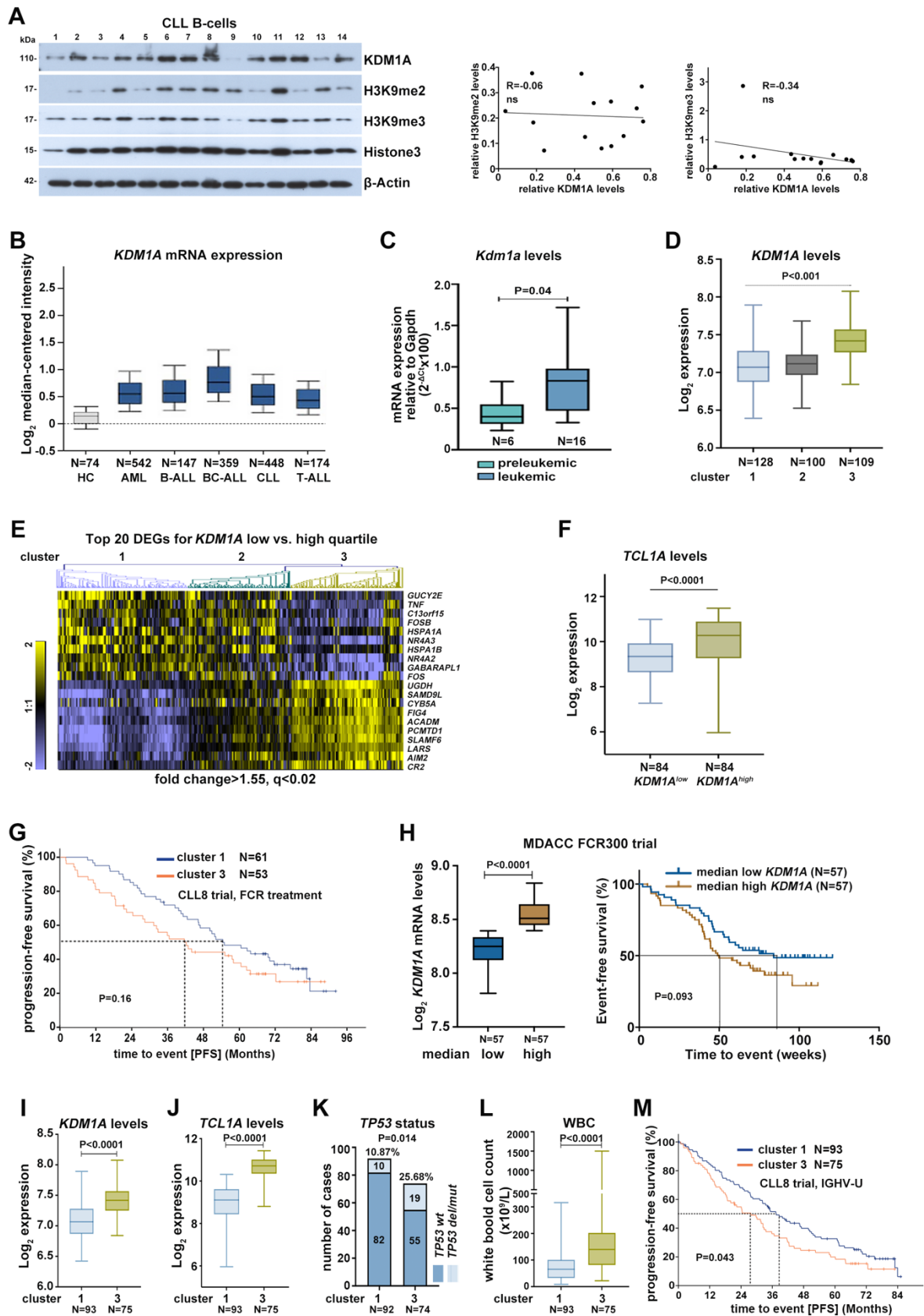
Analysis of GEP data of CLL tumor cells from the CLL8 clinical trial

RNA-seq data processing

ChIP-seq data processing

Supplemental Figures

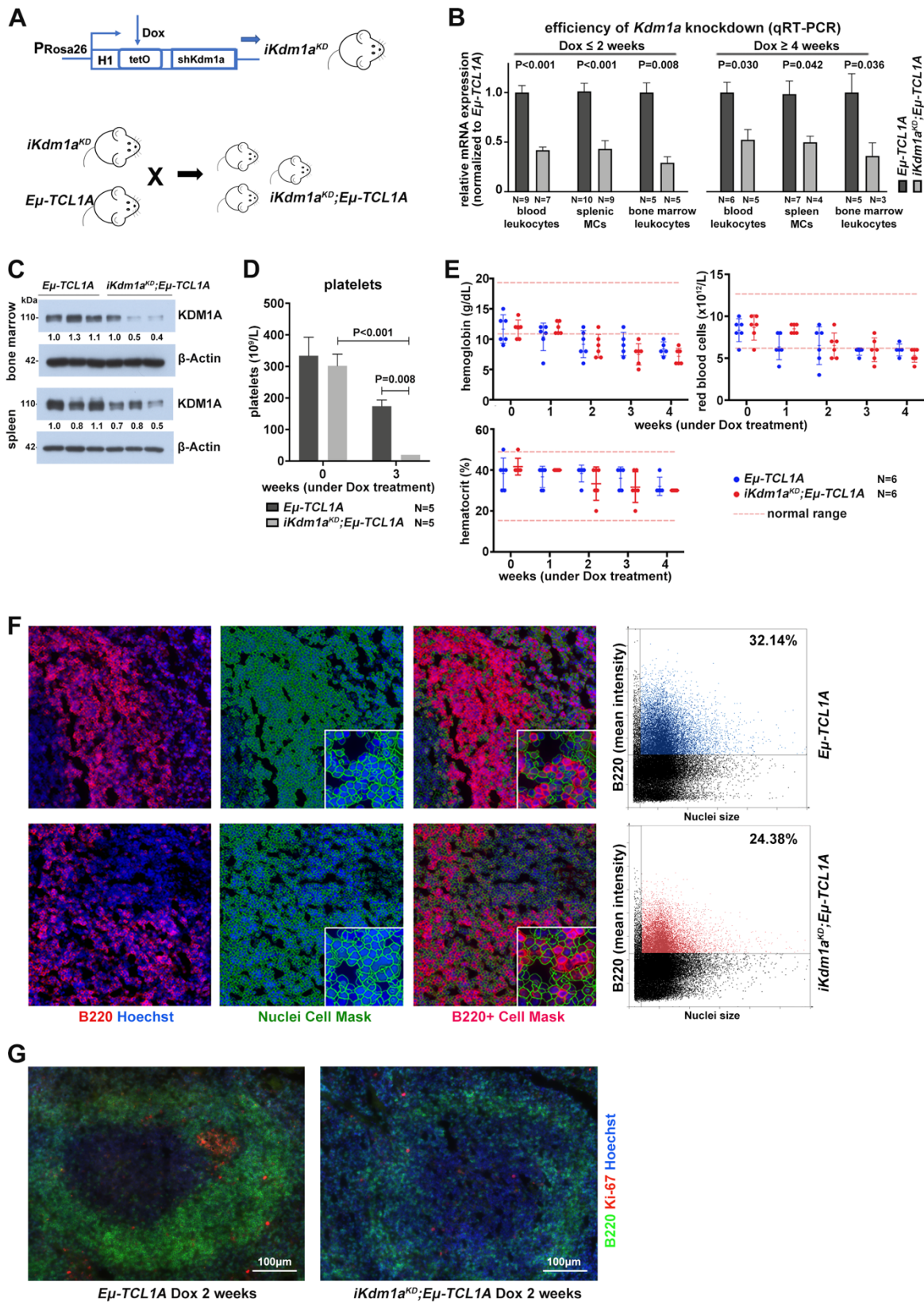
Supplemental Figure 1



Supplemental Figure 1.

(A) Left: immunoblots of KDM1A, H3K9me2, and H3K9me3 in primary CLL cells. Right: no correlation between KDM1A and H3K9me2/me3 protein levels (densitometry values from immunoblots of 14 cases). **(B)** *KDM1A* expression in different lymphatic and myeloid neoplasms as analyzed on Human Genome U133 Plus 2.0 Arrays (Affymetrix) (dataset of Haferlach on www.oncomine.org). Boxes with medians and 25th/75th percentiles. Whiskers show 10th and 90th percentiles. HC, healthy controls. **(C)** Higher *Kdm1a* mRNA levels were detected by qRT-PCR in splenic B-cells of *Eμ-TCL1A* mice at the overt leukemic stages (N=16) vs. those of preleukemic stages (N=6, P=0.04, Mann-Whitney test, boxes & whiskers with median and min-max). **(D)** CLL patients of cluster 3 (clusters defined in **Figure 2E**, N=109) showing significantly higher *KDM1A* expression levels compared to cluster 1 (N=128, P<0.001, Mann Whitney test, box with min-max). **(E)** Heatmap showing the top 10 up or down-regulated genes in CLL patients (N=337) with different *KDM1A* expression levels (low quartile vs. high quartile) as assessed for **Figure 2E** (FCh>1.55, FDR q-value<0.02). **(F)** CLL patients of *KDM1A*^{high} quartile have significantly higher *TCL1A* levels in comparison to *KDM1A*^{low} quartile (N=84 of each quartile, P<0.0001, Mann Whitney test, box with min-max). **(G)** Kaplan-Meier curve showing progression-free survival (PFS) for patients in cluster 1 (N=61, median 55.2 months) and cluster 3 (N=53, median 42.4 months) in the fludarabine / cyclophosphamide / rituximab (FCR) trial arm, HR: 1.318 (95% CI: 0.879-2.172), P=0.16, Log-rank test. **(H)** Validations in the M.D. Anderson Cancer Center (MDACC) FCR300 trial cohort. Left: *KDM1A* levels (array-based gene expression)¹ in the median-based *KDM1A* low vs. high groups. Right: Kaplan-Meier curve illustrating a trend of shorter event-free survival (EFS) for patients with high *KDM1A* levels (N=57, median PFS 49 weeks, orange) as compared to those with low *KDM1A* levels (N=57, median PFS 84.1 weeks, blue; P=0.093, Log-rank test). **(I-M)** IGHV-U CLL cases were clustered into three groups using the top 449 differentially expressed genes in patients with high vs. low *KDM1A* levels (high vs. low quartile). CLL patients of cluster 3 show **(I)** significantly higher *KDM1A* expression levels (P<0.0001, Mann Whitney test), **(J)** higher *TCL1A* transcript levels (P<0.0001, Mann Whitney test), **(K)** higher incidence of *TP53* deletions/mutations (*TP53 del/mut*) (P=0.014, Fisher's exact test; wt: wild type), and **(L)** significantly higher white blood cell (WBC) counts (P<0.0001, Mann Whitney test) as compared to patients of cluster 1. Boxes & whiskers show median and min-max. **(M)** Kaplan-Meier curve illustrating a significantly shorter progression-free survival (PFS) for patients in cluster 3 (median PFS 27.8 months, orange) as compared to those of cluster 1 (median PFS 37.5 months, blue; HR: 1.425 (95% CI: 1.009-2.013), P=0.043, Log-rank test).

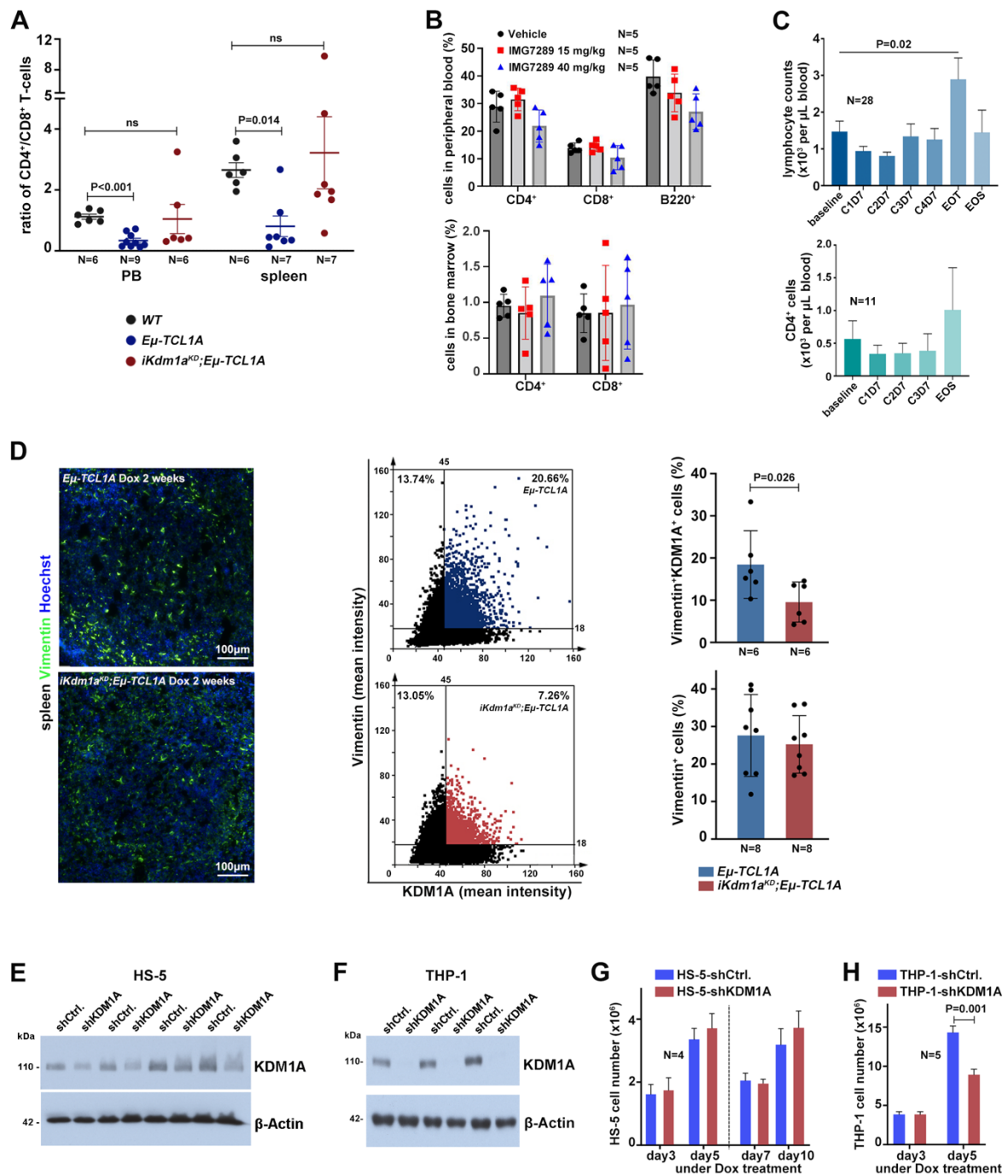
Supplemental Figure 2



Supplemental Figure 2.

(A) Establishment of the inducible *Kdm1a* knockdown mouse model. Top: Schematic representation of the TET-ON system used to induce the *Kdm1a*-specific shRNA in vivo. Bottom: Inducible *Kdm1a* knockdown mice (*iKdm1a^{KD}*) were crossbred with *Eμ-TCL1A* mice to achieve *Kdm1a* knockdown in *Eμ-TCL1A* mice in a Dox inducible manner (*iKdm1a^{KD};Eμ-TCL1A*). **(B)** qRT-PCR analysis demonstrating decreased expression of *Kdm1a* in peripheral blood leukocytes, splenic mononuclear cells (MCs), and bone marrow leukocytes of *iKdm1a^{KD};Eμ-TCL1A* animals (grey) under Dox application for short term (≤ 2 weeks, left) or long term (≥ 4 weeks, right) compared to *Eμ-TCL1A* control mice (dark grey, all $P < 0.05$, Mann Whitney test, Mean \pm SEM). **(C)** Immunoblots showing reduced KDM1A protein levels in bone marrow and spleen of *iKdm1a^{KD};Eμ-TCL1A* mice. Proteins were isolated from bone marrow cells and splenic mononuclear cells of *iKdm1a^{KD};Eμ-TCL1A* and *Eμ-TCL1A* leukemic mice after 2 weeks of Dox treatment. **(D)** Complete blood count test showing reduced platelet counts in peripheral blood of *iKdm1a^{KD};Eμ-TCL1A* mice (N=5, grey) under Dox treatment for 3 weeks in comparison to *Eμ-TCL1A* (N=5, dark grey, $P < 0.001$, Mann Whitney test, Mean \pm SEM). **(E)** No significant difference in peripheral blood erythroid parameters (hemoglobin, red blood cell counts, hematocrit) was found between *Eμ-TCL1A* (N=6, blue) and *iKdm1a^{KD};Eμ-TCL1A* (N=6, red) under Dox treatment. **(F)** An example of tissue cytometry data processing. Spleen sections (top: *Eμ-TCL1A*, bottom: *iKdm1a^{KD};Eμ-TCL1A*) with immunofluorescent staining (B220 red, Hoechst Blue) were scanned at 60x magnification using an IX83 fluorescent invert microscope (Olympus, Japan). Images were processed with StrataQuest using the nuclear marker as the master channel to identify all cells. A secondary measure mask, derived from the nuclear mask, was used to measure cytoplasmic reactivity. For markers expressed in the nucleus (e.g., Ki-67), the nuclear mask was used to quantify the signal. Cutoffs were set interactively using the “forward connection” feature in the software, which links each dot in the scattergram to the corresponding event in the image. **(G)** Representative images of Ki-67 (red) / B220 (green) immunofluorescent stainings in spleen sections (right: *Eμ-TCL1A*, left: *iKdm1a^{KD};Eμ-TCL1A*). Slides with immunofluorescent staining were scanned at 60x magnification using an IX83 fluorescent invert microscope.

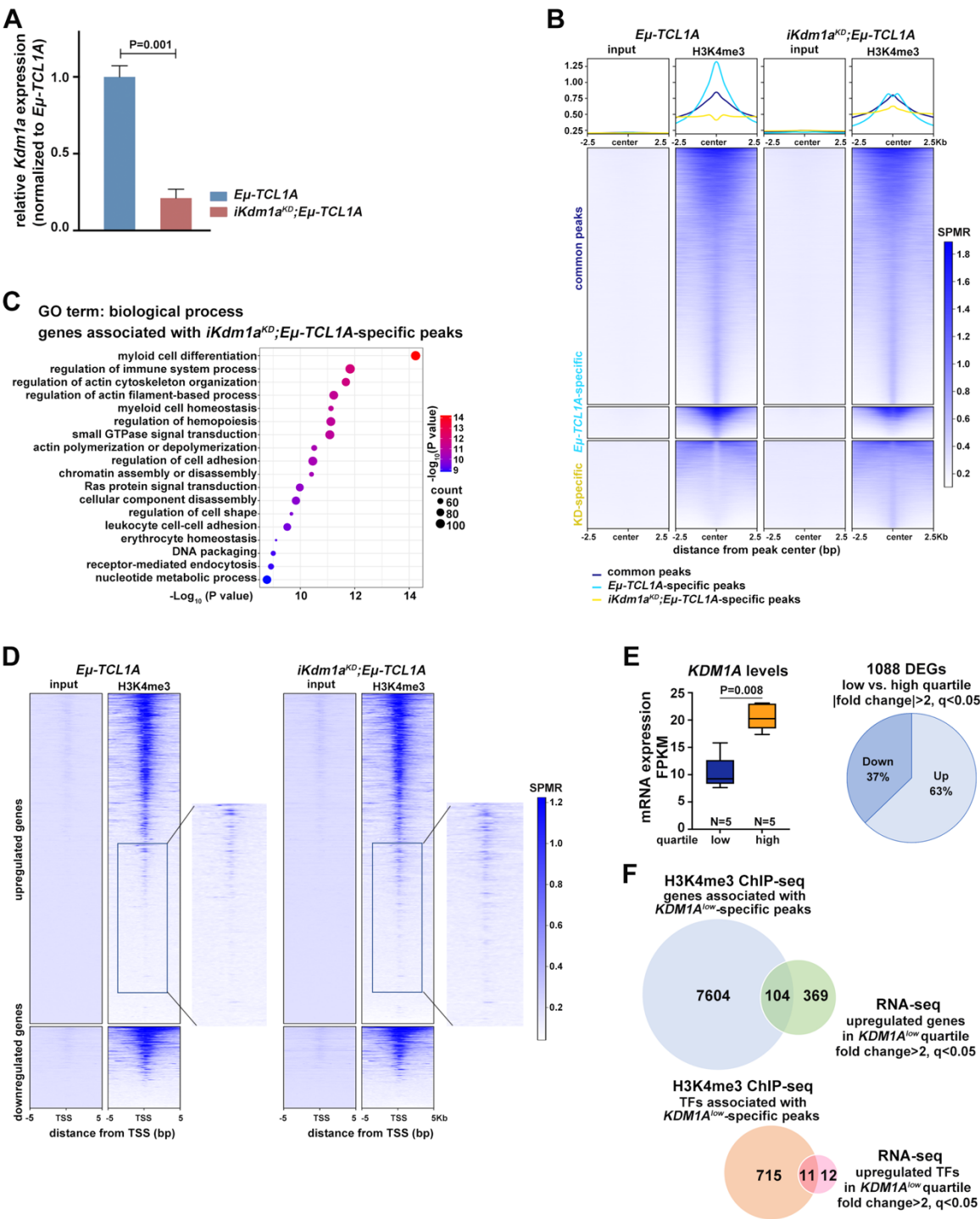
Supplemental Figure 3



Supplemental Figure 3.

(A) Flow cytometric analysis revealing a significantly reduced ratio of CD4⁺/CD8⁺ T-cells in peripheral blood ($P<0.001$) and spleen ($P=0.014$) in *Eμ-TCL1A* leukemic mice but not in *iKdm1a^{KD};Eμ-TCL1A* mice under Dox treatment till the end of the survival analysis, compared to age-matched wild type (*WT*) mice (Mean±SD, Mann Whitney test). ns: not significant. **(B)** C57/BL6 wide-type mice (8 weeks) were treated with vehicle (N=5), 15mg/kg IMG7289 (N=5), or 40mg/kg IMG7289 (N=5) for 7 days. Bar charts showing no significant changes in CD4⁺ or CD8⁺ T-cell population in peripheral blood (top) or in bone marrow (bottom). **(C)** Patients with myelodysplastic syndromes were treated with IMG7289 within the scope of the NCT02842827 clinical trial. Bar chart showing no drop in lymphocyte counts (top, N=28) at the end of treatment and of CD4⁺ T-cells (bottom, N=11) at the end of the study. C: cycle, D: day, EOT: end of treatment, EOS: end of study **(D)** Left: Representative immunofluorescent staining of Vimentin in spleen sections (upper: *Eμ-TCL1A*, lower: *iKdm1a^{KD};Eμ-TCL1A*). Middle: Representative tissue cytometry plots of Vimentin/KDM1A signal (upper: *Eμ-TCL1A*, lower: *iKdm1a^{KD};Eμ-TCL1A*). Right: Quantification of F4/80/KDM1A signal displaying a decrease of KDM1A signal (upper, $P=0.026$) in Vimentin⁺ fibroblasts in spleen sections from *iKdm1a^{KD};Eμ-TCL1A* mice without changes in the cell number (lower) of Vimentin⁺ fibroblasts (Mean±SD, Mann Whitney test). **(E)** Dox-inducible KDM1A knockdown stromal HS-5-shKDM1A cells and control line HS-5-shCtrl. cells were treated with Dox for 7 days. Immunoblots displaying decreased KDM1A levels in HS-5-shKDM1A cell line compared to control cell line. Each pair represents an independent experiment. **(F)** Dox-inducible KDM1A knockdown monocytic THP-1-shKDM1A cells and control line THP-1-shCtrl. cells were treated with Dox for 5 days. Immunoblots showing reduced KDM1A levels in THP-1-shKDM1A cell line vs. control cells. Each pair represents an independent experiment. **(G)** Bar charts showing no significant differences in cell count of HS-5-shCtrl. (blue) and HS-5-shKDM1A (red) cells under Dox treatment (N=4 independent experiments). **(H)** Bar charts illustrating significantly lower cell count of THP-1-shKDM1A (red) cells after 5 days of Dox treatment compared to the control cell line (blue; N=5 independent experiments. $P=0.001$, Mann Whitney test, Mean±SEM).

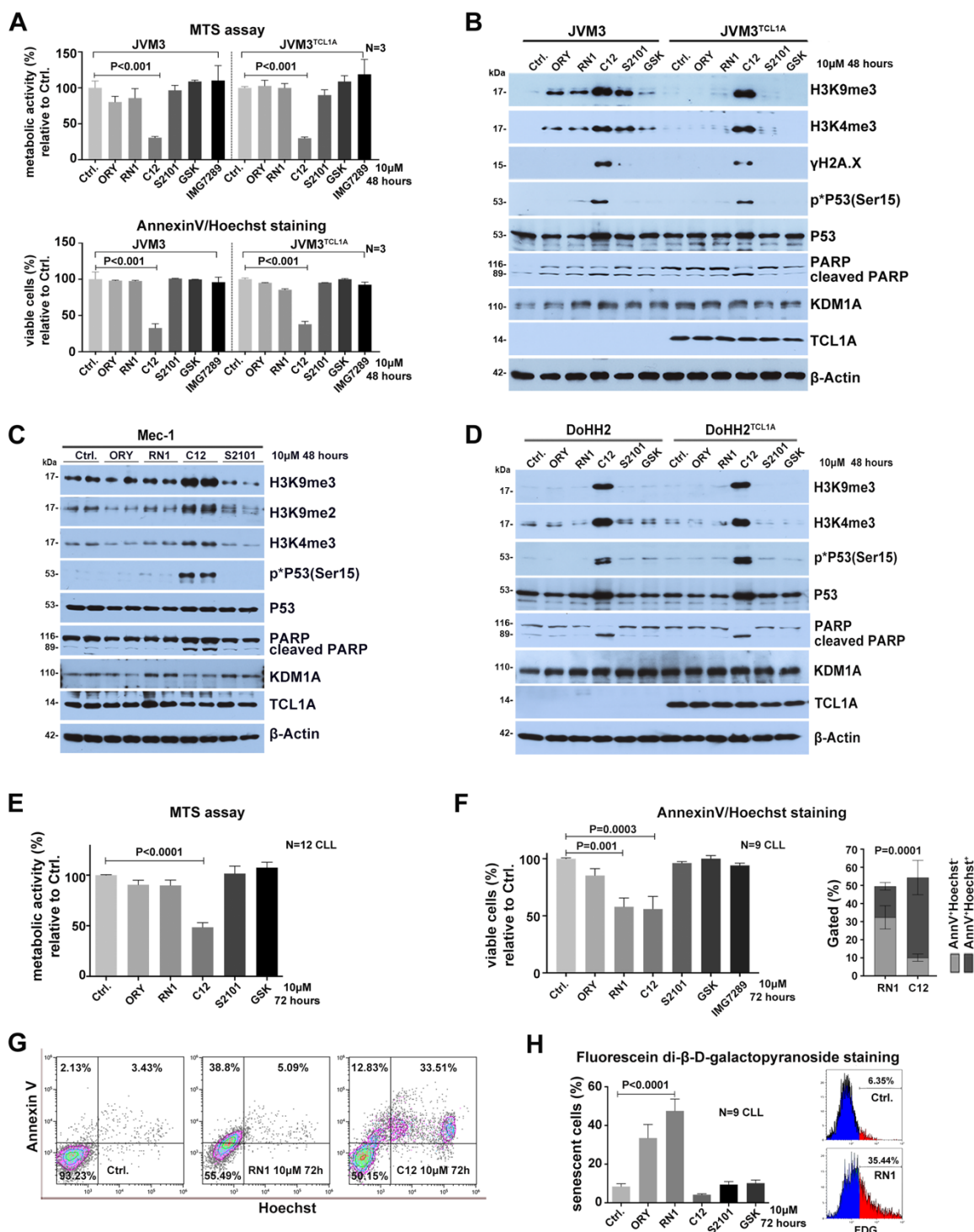
Supplemental Figure 4



Supplemental Figure 4.

(A) qRT-PCR analysis demonstrating significantly reduced expression of *Kdm1a* in splenic mononuclear cells of *iKdm1a^{KD};Eμ-TCL1A* in comparison to *Eμ-TCL1A* mice included in the CHIP experiments (N=3 animals of each group. Mean±SEM, P=0.001, Mann Whitney test). **(B)** H3K4me3 binding occupancy at common and specific regions in *Eμ-TCL1A* and *iKdm1a^{KD};Eμ-TCL1A* splenocytes. Signal is displayed from -2.5 kb to +2.5 kb surrounding the center of each peak. SPMR: signal per million reads. **(C)** Gene ontology (GO) analysis of genes associated with *iKdm1a^{KD};Eμ-TCL1A*-specific H3K4me3 regions. Bubble plot showing the enriched biological processes. **(D)** H3K4me3 binding occupancy at regions of differentially expressed genes in *Eμ-TCL1A* and *iKdm1a^{KD};Eμ-TCL1A* splenic mononuclear cells. Signal is displayed from -5 kb to +5 kb from the transcription start site (TSS). **(E)** Left: Publicly available RNA-seq data (GEO dataset: GSE113336) of 19 CLL cases were analyzed. Boxes showing the *KDM1A* mRNA levels of low and high quartiles (N=5 cases per group). Right: Pie chart showing 63% of 1088 differentially expressed genes (DEGs) to be upregulated in the *KDM1A^{low}* group. **(F)** Publicly available H3K4me3-ChIP-seq and RNA-seq data (GEO dataset: GSE113336; EGA dataset: EGAD00001003421) of 19 CLL cases were analyzed. Top: Venn diagram showing the overlap of genes associated with *KDM1A^{low}*-specific H3K4me3 regions with genes upregulated in the *KDM1A^{low}* group (RNA-seq data; fold change >2, q<0.05). Bottom: Venn diagram showing the overlap of transcription factor (TF)-encoding genes annotated to *KDM1A^{low}*-specific H3K4me3 peaks and TF-encoding genes upregulated in *KDM1A^{low}* group (RNA-seq data; fold change >2, q<0.05).

Supplemental Figure 5

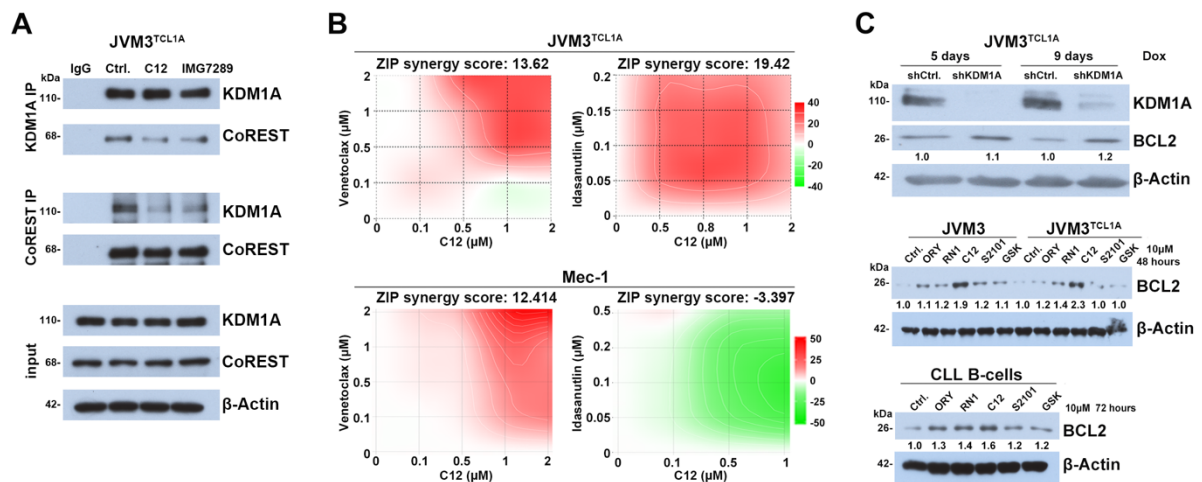


Supplemental Figure 5.

(A) Metabolic activity (MTS assay, top) and percentage of viable cells (AnnexinV/Hoechst flow cytometry, bottom), in JVM3^{±TCL1A} cells treated with KDM1A inhibitors (10μM) for 48 hours. The inhibitor C12 markedly reduced metabolic activity ($P < 0.001$) and viability ($P < 0.001$) of JVM3^{±TCL1A} cells as compared to controls (3 independent experiments, Student's t-test,

Mean±SEM). **(B)** Representative immunoblots displaying induction of apoptosis as shown by phosphorylation of P53 and cleavage of PARP alongside an increase in tri-methylation of H3K4/9 by C12 in both JVM3^{±TCL1A} sublines (3 independent experiments). **(C)** CLL-like Mec-1 cells were treated with selected KDM1A inhibitors (10μM) for 48 hours. Representative immunoblots displaying induction of apoptosis as shown by phosphorylation of P53 and cleavage of PARP alongside an increase in tri-methylation of H3K4/9 by C12 in Mec-1 cells (two lanes for each condition represent technical replicates, N=3 independent experiments). **(D)** DoHH2^{±TCL1} cells were treated with selected KDM1A inhibitors (10μM) for 48 hours. Representative immunoblots showing induction of apoptosis as shown by phosphorylation of P53 and cleavage of PARP, and increased tri-methylation of H3K4/9 by treatment with C12 in both TCL1A negative and positive DoHH2 cells (N=3 independent experiments). **(E-H)** Primary CLL cells were co-cultured with differentiated THP-1 cells supplemented with CpG and IL-15 for 36 hours. Samples with >35% Ki-67⁺ cells were selected and subsequently treated with KDM1A inhibitors (10μM) for 72 hours (selected samples listed in **Supplemental Table 12**). **(E)** C12 decreased the metabolic activity of CLL cells as per MTS assay (N=12 CLL, P<0.001, Student t-test, Mean±SEM). **(F)** Left: The inhibitors C12 and RN1 compromised CLL cell viability (AnnexinV/Hoechst flow cytometry, N=9 CLL, both P<0.05, Student's t-test, Mean±SEM). Right: more AnnexinV⁺/Hoechst⁻ (grey) and less AnnexinV⁺/Hoechst⁺ (dark grey) cells in RN1-treated CLL samples as compared to C12 treatment (N=12, P=0.0001, a two-way ANOVA, Mean±SEM). **(G)** Representative flow cytometry plots (AnnexinV/Hoechst) in CLL samples. Left: 93.23% viable cells (double-negative) in vehicle-exposed control condition. Middle: RN1 treatment induced early apoptotic changes (AnnexinV⁺/Hoechst^{negative}). Right: exposure to C12 evoked marked apoptotic cell death (AnnexinV⁺/Hoechst⁺). **(H)** Left: Particularly RN1 promoted cellular senescence in human CLL samples (N=9) as per flow-cytometric Di-β-D-Galactopyranoside (FDG) staining (P=0.002, Student's t-test, Mean±SEM). Right: FDG flow cytometry plots in a representative CLL sample (control and RN1 treatment).

Supplemental Figure 6



Supplemental Figure 6.

(A) Immunoblots of co-IPs using IgG or KDM1A or CoREST antibodies illustrating lower abundances of KDM1A-CoREST interactions in JVM3^{TCL1A} cells treated with C12 or with IMG7289. **(B)** JVM3^{TCL1A} and Mec-1 cells were treated with C12 plus venetoclax or idasanutlin at indicated concentrations for 48 hours with cell viability assessed via AnnexinV/Hoechst flow cytometry. Synergistic effects were calculated using SynergyFinder based on zero-interaction potency (ZIP).² Top: Two-dimensional contour plots showing the synergistic activity of the combination of C12 with venetoclax (left, ZIP synergy score 13.62) and of C12 with idasanutlin (right, ZIP synergy score 19.42) in JVM3^{TCL1A} leukemic B-cells. Bottom: Two-dimensional contour plots showing the synergistic activity of the combination of C12 with venetoclax (left, ZIP synergy score 12.414) in Mec-1 cells. C12 and idasanutlin did not show synergistic effects (right). **(C)** Immunoblots showing upregulation of BCL2 protein levels upon KDM1A knockdown in JVM3^{TCL1A} cells (top), and after treatment with the indicated KDM1A inhibitors in JVM3 cells (middle) and primary CLL cells (bottom). Top: JVM3^{TCL1A}-shCtrl. and JVM3^{TCL1A}-shKDM1A cells were exposed to doxycycline for 5 days and 9 days to induce *KDM1A* knockdown. Middle and bottom: JVM3 cells and primary CLL cells were treated with 10μM KDM1A inhibitors for 48 hours or 72 hours, respectively.

Supplemental Methods

Isolation of B-cells from tonsils

Tonsillar B-cells were isolated from human reactive tonsils. After homogenizing, the tonsils were digested with collagenase NB4 (Serva) for 2h. After filtering, washing, and supplementation with red blood cells (RBCs, ratio of 100 RBCs per nucleated cell), the B-cells were enriched using the RosetteSep™ Human B-Cell Enrichment Kit (StemCell Technologies) according to the manufacturer's instructions (purity >90%).

Animal experiments

The mice were bred and housed in animal facilities of the University Hospital of Cologne (Cologne, Germany) under specific pathogen-free conditions. Both *Eμ-TCL1A* and *iKdm1a^{KD};Eμ-TCL1A* groups were from the same breedings (i.e., cross-breeding of *Eμ-TCL1A* and *iKdm1a^{KD}* mice). To assess the effect of *Kdm1a* knockdown in murine CLL, *iKdm1a^{KD};Eμ-TCL1A* and *Eμ-TCL1A* (as control) mice were treated with doxycycline (Dox)-containing diet (1 mg Dox/kg diet, Ssniff).

For determination of disease-specific overall survival and evaluation of disease progression, *iKdm1a^{KD};Eμ-TCL1A* and *Eμ-TCL1A* leukemic mice (white blood cell (WBC) counts $\geq 50 \times 10^3$ / μ L) were fed with the Dox-diet and monitored (blood sampling every week) until the endpoint of survival experiment (Figure 3B-E, 3G, 4A, 4D. Supplemental Figure 2B, 2D-E, 3A). Survival was defined as the days from the start of Dox treatment until the clinical endpoint (a. sustained or rapid weight loss of 20% or 15% over 72 hours; b. significant abdominal distension or ascites burden greater than 10% of body weight; c. bloody or mucous discharge from any natural orifice; d. difficulty in breathing; e. paralysis or weakness of hind limbs; f. significant reduction of movement; g. enlarged lymph nodes or spleen; h. WBCs $> 100 \times 10^9$ /L). For the analysis of apoptotic B-cells in the spleen and the in vitro co-culture of murine leukemic cells with bone marrow stromal cells, both types of cells were isolated from leukemic mice exposed to Dox for 2 weeks (Figure 3I, 4F).

For tissue cytometry, spleens were extracted from *Eμ-TCL1A* and *iKdm1a^{KD};Eμ-TCL1A* leukemic mice fed with Dox-diet for 2 weeks when WBC $\geq 30 \times 10^3$ / μ L (Figure 3F, 3H, 4B-C, 4E. Supplemental Figure 2F-G, 3B).

For RNA-seq and ChIP-seq, splenic mononuclear cells were isolated from *Eμ-TCL1A* and *iKdm1a^{KD};Eμ-TCL1A* leukemic mice (RNA-seq WBC $\geq 30 \times 10^3$ / μ L, ChIP-seq WBC $\geq 80 \times 10^3$ / μ L) treated with Dox for 2 weeks.

Magnetic resonance imaging (MRI) and spleen volumetry

MRI was performed in *Eμ-TCL1A* and *iKdm1a^{KD};Eμ-TCL1A* leukemic mice using an 3.0T Ingenia (Philips) MRI scanner and a specific 40mm diameter solenoid coil for rodents (Philips) equipped with a heating system to prevent cooling of the anesthetized animals. Inhalation of 1.5-2.5% Isoflurane (Abbvie) was used for anesthesia. To obtain images with anatomic details, high-resolution transversal and coronal T2-weighted MR images of the abdomen were acquired. Spleen volumetry was conducted using OsiriX lite (Pixmeo). Volumes were determined by marking the splenic region of interest (ROI) in each section. The spleen volume was determined by the function “ROI Volume” calculating the respective volume in cm³.

Isolation of murine splenic mononuclear cells and bone marrow cells

Mice were killed by cervical dislocation and spleens were excised. Spleen cells were isolated from murine spleens by straining the spleen tissue through a 100 μm cell strainer with a syringe plunger and DPBS (Gibco). Afterwards, a density gradient was carried out to purify the mononuclear cells. For the isolation of bone marrow, a 20 gauge needle was inserted into the growth plate of the femora/Tibia and the bone marrow was removed by flushing with DPBS. Bone marrow was strained through a 100 μm cell strainer with a syringe plunger to obtain a single-cell suspension.

Tissue cytometry

Immunofluorescent staining was performed on 6μm cryosections of murine spleens. Sections were fixed in 4% formaldehyde, followed by antigen retrieval in 1mM EDTA, and blocking with blocking reagent (PerkinElmer). Primary and secondary antibodies (**Supplemental Table 4**) were applied according to standard procedures. Hoechst dye was used for nuclear counter-staining. Slides were scanned using an IX83 motorized inverted fluorescence microscope (Olympus). Visual slides were computed and analyzed using the image cytometry software StrataQuest (TissueGnostics).

Cell culture

HEK293T, HS-5, and primary murine bone marrow stromal cells were cultured in DMEM medium (Gibco) supplemented with 10% fetal bovine serum (Gibco). DoHH2^{±TCL1A}, JVM3^{±TCL1A}, Mec-1, and THP-1 (all DSMZ), primary CLL cells, and murine splenic mononuclear cells were cultured in RPMI-1640 (Gibco) supplemented with 10% fetal bovine serum. Cell culture was done in an incubator (Heraeus) at 37 °C with 5% CO₂. To differentiate THP-1 monocytes into macrophages, cells were cultured for 72 hours at a phorbol 12-myristate 13-acetate (PMA) concentration of 150 nM. To induce proliferation of CLL cells, cells were cocultured with differentiated THP-1 macrophages supplemented with 10 ng/mL recombinant human IL15 (rh IL15, PeproTech) and 0.25 nM CpG (TIB Molbiol) for 36hours. Murine leukemic cells were

cocultured with murine bone marrow stromal cells supplemented with 10 ng/mL recombinant mouse IL15 (rm IL15, PeproTech) and 0.25 nM CpG (TIB Molbiol).

The inhibitors used in combination screens with KDM1A inhibition (JAK3: tofacitinib, STAT5: SH-4-54, PI3K: idelalisib, and PRMT: EPZ015666) were purchased from Selleckchem.

Constructs

Knockdown of KDM1A in cell lines was carried out via RNA interference in a Dox inducible manner. The sequence of shRNA was synthesized (ThermoFisher) and subcloned into the Tet-pLKO-puro vector (Addgene, 21915). The shRNA target sequences were: non-target control, 5'-AGGTAGTGTAAATCGCCTTGTT-3'; KDM1A, 5'-AGCAATACTCGAGTATTGCTA-3'. Constructs were confirmed by Sanger sequencing.

Transfection and transduction

Lentiviral transduction of the Tet-pLKO-puro vectors was performed to generate cells stably expressing the control and KDM1A targeting shRNAs. HEK293T cells were co-transfected with the 2nd generation packaging vectors (pMD2.G and psPAX2, Addgene) and transfer vector using TurboFect reagent (ThermoFisher) according to the manufacturer's instructions. The supernatant (virus) was collected and filtered at 48 hours and 72 hours. The filtered supernatant was mixed 1:1 with the complete culture medium supplemented with 8 µg/mL polybrene (Sigma) and applied to transduce cells. Selection with puromycin (PAA Laboratories) was started 48 hours after transduction (1 µg/mL puromycin for HS-5 selection and 5 µg/mL puromycin for THP-1 selection). shRNA expression was induced by 1 µg/mL Dox (Sigma).

Proliferation assay

To assess cell proliferation, cells were labeled with the cell proliferation dye eFluor 670 (eBioscience) following the manufacturer's instructions. Loss of eFluor 670 was assessed by flow cytometry as indicative of cell proliferation.

Demethylase activity assay

In cell lines, KDM1A demethylase activity assay was performed using the EpiQuick histone demethylase LSD1 Activity/Inhibition Assay Kit (Epigentek) according to the manufacturer's instructions. Briefly, 2-8µg nuclear protein extracted with the Nuclear Extraction Kit (Ab113474; Abcam) was incubated with the KDM1A substrate. The substrate that has not been demethylated by KDM1A was recognized by staining with a specific antibody, followed by incubation with the detection antibody. The amount of un-demethylated products, which is inverse proportional to KDM1A activity, then was measured by reading the fluorescence. The activity of KDM1A was inversely proportional to the fluorescent intensity measured. The demethylase activity was calculated using the formula below. RFU: relative fluorescent unit.

$$\text{Activity (RFU/hour/}\mu\text{g)} = \frac{\text{RFU (control - blank)} - \text{RFU (sample - blank)}}{\text{reaction time (hour)} \times \text{protein amount (}\mu\text{g)}}$$

In primary CLL cells, KDM1A activity assay was performed using the KDM1A Activity Quantification Assay Kit (Fluorometric; Abcam) according to the manufacturer's instructions. Briefly, 2-10 μ g nuclear protein extracted with the Nuclear Extraction Kit (Ab113474; Abcam) was incubated with the KDM1A substrate. The KDM1A-demethylated products was recognized by staining with a specific antibody, followed by incubation with the detection antibody. The amount of demethylated products, which is proportional to enzyme activity, was measured by reading the fluorescence.

MTS assay

MTS assay was performed using CellTiter 96® Aqueous One Solution MTS Assay (Promega) according to the manufacturer introductions. 100 μ L of cell suspension and 20 μ L of substrate were added to each well and plates were incubated at 37 °C for 0.5-3 hours in a humidified, 5% CO₂ incubator. Measurements were made in triplicates per condition. Absorbance was recorded at 490 nm using Spectramax Paradigm (BeckmanCoulter).

Chromatin immunoprecipitation sequencing (ChIP-seq)

The SimpleChIP enzymatic chromatin IP Kit (Cell Signaling) was used according to the manufacturer's instructions. Briefly, splenocytes were fixed in 1% formaldehyde for 9min at room temperature. After quenching with glycine, cells were lysed and chromatin was nuclease treated followed by shearing via sonication. Anti-H3K4me3 (#9751, Cell Signaling) antibodies were used for ChIPs. After reverse cross-linking and DNA purification, ChIP-DNA and whole nuclear DNA (control) were subjected to library preparation and sequenced on an Illumina NovaSeq 6000 device.

Quantitative real-time PCR (qRT-PCR)

qRT-PCR was carried out on a 7500 FAST Real-Time PCR System (Applied Biosystems) using GoTag® SYBR green qPCR Master Mix (Promega). Primer sequences (Metabion) are listed in the table below. The murine mRNA expression levels were normalized to Gapdh levels.

Primers used for qPCR:

Target	Species	Primer Sequence 5' → 3'
KDM1A (qRT-PCR)	human	forward: TCGGGTGTTCTGGGATCCAAGTGT reverse: ATCGGCCAACAAATCACATCGTCAC
ACTB (qRT-PCR)	human	forward: GACAGGATGCAGAAGGAGAT reverse: TTGCTGATCCACATCTGCTG
Cxcr4 (qRT-PCR)	mouse	forward: GACTGGCATAGTCGGCAATG reverse: AGAAGGGGAGTGTGATGACAAA

Gapdh (qRT-PCR)	mouse	forward: TGGCCTTCCGTGTTCTCTAC reverse: GAGTTGCTGTTGAAGTCGCA
Itgb2l (qRT-PCR)	mouse	forward: ACTGTCTCAGTTGTGTACCAAG reverse: GCTCTGGTGTATCACAGCGAA
Kdm1a (qRT-PCR)	mouse	forward: GGCGCAAGCGGGCCAAGGTAGA reverse: GACGGCTCTTCCGGCTCACTTTCA
Rapgef3 (qRT-PCR)	mouse	forward: TCTTACCAGCTAGTGTTCGAGC reverse: AATGCCGATATAGTCGCAGATG

Mass spectrometry (MS)

For liquid chromatography (LC)-MS/MS experiments of primary samples, cell lysates from 11 CLL samples (N=11) and B-cells isolated from reactive tonsils (N=3) were immunoprecipitated using Protein G Sepharose beads (Sigma) coupled to specific anti-TCL1A antibodies (clone 1-21).³ Immunoprecipitation (N=3 CLL) with unspecific IgGs were used as the negative control. Each sample was done in two technical replicates. Eluates were analyzed by LC-MS/MS as described previously.⁴ The eluted proteins were precipitated, resuspended in 8 M Urea (Sigma), reduced in 5 mM dithiothreitol (Applichem), and alkylated in 10 mM iodoacetamide (Sigma). Protein digestions were performed with endoproteinase Lys-C (4h, WAKO Chemicals, Richmond, USA) and subsequently trypsin (16h, Serva) at an enzyme:substrate ratio of 1:100. The digested peptides were purified by using a C18 stage tip (self-made by using a double-layer of AttractSPE Disks Bio SDB-RPS, Affiniseq) and analyzed by LC-MS/MS on an LTQ Orbitrap Discovery mass spectrometer (ThermoFisher) in the CECAD proteomics core facility. A label-free quantification (LFQ) algorithm was applied to quantitatively determine the peptide enrichment in measured samples.

For Histone post-transcriptional modification (PTM) MS, total histones were extracted from isolated nuclei by standard acid extraction.⁵ The extracted histones were trypsinized and subjected to two rounds of propionylation. The resulting derivatized peptides were desalted using C18 Stage Tips and subjected to nLC-MS/MS for comprehensive quantitation of PTMs and analyzed on an Orbitrap Fusion Tribrid mass spectrometer (ThermoFisher).

Analysis of MS data

For the analysis of the TCL1A interactome in primary CLL cells, the Perseus software (Max Planck Society) was used. Proteins with less than 25 valid values among all samples were sorted out and missing values were replaced by random numbers based on a normal distribution (width 0.3; downshift: 1.8). To identify specific TCL1A interacting proteins, a Welch test was performed, comparing the log₂ of LFQ intensities of the different groups with the log₂ of LFQ intensities of IgG (fold change >2, q <0.05). The identified TCL1A interactome within each group was subsequently compared between the different groups using a Welch test (fold change >2, q <0.05). The MS-based proteomics data are deposited at the ProteomeXchange

Consortium via the PRIDE33 partner repository with the dataset identifier PXD029961 (Reviewer account details: Username: reviewer_pxd030773@ebi.ac.uk, password: b2Cx0OLM).

For histone PTM MS, data were acquired using a data-independent acquisition method (DIA) and analyzed using EpiProfile v.2.0.⁶ The peptide relative ratio was calculated using the total area under the extracted ion chromatograms of all peptides with the same amino acid sequence with all modified forms as 100%. For isobaric peptides, the relative ratio of two isobaric forms was estimated by averaging the ratio for each fragment ion with a different mass between the two species. Raw data are available at the Chorus repository (<https://chorusproject.org/>) under project number 1743.

Analysis of GEP data of CLL tumor cells from the CLL8 clinical trial

The expression intensities derived from the Affymetrix GeneChip® Human Exon 1.0 ST Array were restricted to “core” probe sets and averaged on gene levels. The robust multi-array average (RMA) algorithm providing a log₂-transformed summary measure of gene expression was used for data normalization. Differential gene expression was calculated by using a univariate permutation test with the Benjamini-Hochberg correction for multiple testing. Agglomerative hierarchical clustering was done by using Pearson’s correlation coefficient for distance measures and average linkage as agglomeration rules. The Affymetrix Power Tools (http://www.affymetrix.com/partners_programs/programs/developer/tools/powertools.affx) and BRB-Array tools (<http://linus.nci.nih.gov/BRB-ArrayTools.html>) were used for analyses, including normalization. The genesis clustering software was used for clustering and visualization. Data were submitted to the Gene Expression Omnibus (GEO) database under accession number GSE126595.

RNA-seq data processing

RNA-seq data of murine samples were processed using a high-throughput Next-Generation Sequencing analysis pipeline.⁷ FastQC (v0.10.1) was used for basic read quality check and read statistics were acquired with SAMtools v0.1.19.⁸ Reads were mapped to the mouse reference (version 93) using Tophat v2.0.10,⁹ and gene quantification was carried out using a combination of Cufflinks v2.1.1,¹⁰ and the DESeq2 package v1.4.5,¹¹ with genomic annotation from the Ensembl database, version 93. The results were uploaded into an in-house MySQL database and joined with BiomaRt v2.20.0¹² annotations from Ensembl, version 93. Lists of differentially expressed genes were defined by a final database export using 5 and 0.01 as cutoffs for DESeq2-based fold changes and p-values, respectively. Data were submitted to the GEO database under accession number GSE190108.

Publicly available RNA-seq data (GEO dataset: GSE113336; EGA dataset: EGAD00001003421)¹³ of 19 CLL cases were mapped using STAR v2.7.8a¹⁴ and gencode gene annotation v13. Read counts were collected with RSEM v 1.3.1¹⁵ and differential expression analysis was done with edgeR v3.38.4.¹⁶

ChIP-seq data processing

ChIP-seq reads of murine samples were mapped to a mouse reference genome provided by the Mouse Genome Reference Consortium (GRCm39/mm39) / using Bowtie2 v. 2.2.9,¹⁷ and aligned reads from biological replicates were pooled together. Peaks were called for pooled samples with MACS2 v. 2.2.6¹⁸ using the corresponding inputs and default parameters. Differential peaks were identified using MACS2 bdgdiff default parameters. Heatmaps and average profile plots were generated using coverage normalized to signal per million reads (SPMR) using deeptool.¹⁹ Peak annotation according to GENCODE gene annotation vM27 of the corresponding peaks sets was performed using annotatePeaks.pl function of HOMER v4.11.1²⁰ and custom R 4.0.0 scripts. Analysis of transcription factor motifs at each peak set was performed using findMotifsGenome.pl of HOMER v4.11.1.²⁰ Data were submitted to the GEO database under accession number GSE188536. To review it, please use the secure token “mpsvequeuvhefjgl”.

Publicly available ChIP-seq data (GEO dataset: GSE113336; EGA dataset: EGAD00001003421)¹³ of 19 CLL cases were mapped to a human reference genome provided by Human Genome Reference Consortium (GRCh37/hg19) using Bowtie2 v. 2.2.9,¹⁷ and aligned reads from each group were pooled together. Peaks were called for pooled samples with MACS2 v. 2.2.6¹⁸ using the corresponding inputs and default parameters. Differential peaks were identified using MACS2 bdgdiff default parameters. Peak annotation according to GENCODE gene annotation v13 of the corresponding peaks sets was performed using annotatePeaks.pl function of HOMER v4.11.1²⁰ and custom R 4.0.0 scripts.

References:

1. Herling CD, Coombes KR, Benner A, et al. Time-to-progression after front-line fludarabine, cyclophosphamide, and rituximab chemoimmunotherapy for chronic lymphocytic leukaemia: a retrospective, multicohort study. *Lancet Oncol.* 2019;1576-1586.
2. Ianevski A, Giri AK, Aittokallio T. SynergyFinder 2.0: Visual analytics of multi-drug combination synergies. *Nucleic Acids Research.* 2021;48(1):W488-W493.
3. Herling M., Patel K., Khalili J. et al. TCL1 shows a regulated expression pattern in chronic lymphocytic leukemia that correlates with molecular subtypes and proliferative state. *Leukemia.* 2006;20:280-285.
4. Cox J, Hein MY, Luber CA, et al. Accurate proteome-wide label-free quantification by delayed normalization and maximal peptide ratio extraction, termed MaxLFQ. *Mol Cell Proteomics.* 2014;13(9):2513-26.
5. Karch KR, Sidoli S, Garcia BA. Identification and Quantification of Histone PTMs Using High-Resolution Mass Spectrometry. *Methods Enzymol.* 2016;574:3-29.
6. Yuan ZF, Sidoli S, Marchione DM, et al. EpiProfile 2.0: A Computational Platform for Processing Epi-Proteomics Mass Spectrometry Data. *J Proteome Res.* 2018;17(7):2533-2541.
7. Wagle P, Nikolić M, Frommolt P. QuickNGS elevates Next-Generation Sequencing data analysis to a new level of automation. *BMC Genomics.* 2015;16(1):487.
8. Li H, Durbin R. Fast and accurate short read alignment with Burrows-Wheeler transform. *Bioinformatics.* 2009;25(14):1754-60.
9. Trapnell C, Pachter L, Salzberg SL. TopHat: discovering splice junctions with RNA-Seq. *Bioinformatics.* 2009;25(9):1105-11.
10. Trapnell C, Williams BA, Pertea G, et al. Transcript assembly and quantification by RNA-Seq reveals unannotated transcripts and isoform switching during cell differentiation. *Nat Biotechnol.* 2010;28(5):511-5.
11. Anders S, Huber W. Differential expression analysis for sequence count data. *Genome Biol.* 2010;11(10):R106.
12. Durinck S, Moreau Y, Kasprzyk A, et al. BioMart and Bioconductor: a powerful link between biological databases and microarray data analysis. *Bioinformatics.* 2005;21(16):3439-40.
13. Mallm J, Iskar M, Ishaque N, et al. Linking aberrant chromatin features in chronic lymphocytic leukemia to transcription factor networks. *Mol Syst Biol.* 2019;15(5):1-20.
14. Dobin A, Davis CA, Schlesinger F, et al. STAR: ultrafast universal RNA-seq aligner. *Bioinformatics.* 2013;29(1):15-21.
15. Li B, Dewey CN. RSEM: accurate transcript quantification from RNA-Seq data with or without a reference genome. *BMC Bioinformatics.* 2011;12:323.
16. Robinson MD, McCarthy DJ, Smyth GK. edgeR: a Bioconductor package for differential expression analysis of digital gene expression data. *Bioinformatics.* 2010;26(1):139-40.
17. Langmead B, Salzberg SL. Fast gapped-read alignment with Bowtie 2. *Nat Methods.* 2012;9(4):357-9.
18. Zhang Y, Liu T, Meyer CA, et al. Model-based analysis of ChIP-Seq (MACS). *Genome Biol.* 2008;9(9):R137.
19. Ramírez F, Ryan DP, Grüning B, et al. deepTools2: a next generation web server for deep-sequencing data analysis. *Nucleic Acids Res.* 2016;44(W1):W160-5.

20. Heinz S, Benner C, Spann N, et al. Simple combinations of lineage-determining transcription factors prime cis-regulatory elements required for macrophage and B cell identities. *Mol Cell*. 2010;38(4):576-89.